Influence of BSA adsorption on the oxide layers developed on 70Cu-30Ni alloy in static artificial seawater

B. Torres, A. Seyeux, S. Zanna, Bernard Tribollet, P. Marcus, Isabelle Frateur

Matériaux & Techniques **101**, 106 (2013)

DOI: 10.1051/mattech/2013059
www.mattech-journal.org

Matériaux & Techniques

Influence of BSA adsorption on the oxide layers developed on 70Cu-30Ni alloy in static artificial seawater*

B. Torres[1], A. Seyeux[1], S. Zanna[1], B. Tribollet[2], P. Marcus[1] and I. Frateur[1,2]

Received 16 July 2012, Accepted 15 February 2013

Abstract – Copper alloys usually used in cooling circuits of industrial plants can be affected by biocorrosion induced by biofilm formation. The global objective is to study the influence of biomolecules adsorption, which is the first step in biofilm formation, on the electrochemical behaviour of 70Cu-30Ni (wt. %) alloy and the chemical composition of oxide layers. In this work, the chosen biomolecule was the bovine serum albumin (BSA, model protein) and electrochemical measurements performed after 1 h of immersion in static artificial seawater were combined to surface analyses. In the presence of BSA, the charge transfer resistance deduced from EIS data at E_{corr} is higher, corresponding to lower corrosion current. Without BSA, two oxidized layers are shown by XPS and ToF-SIMS: an outer layer mainly composed of copper oxide (Cu_2O redeposited layer) and an inner layer mainly composed of oxidized nickel, with a global thickness of ∼30 nm. The presence of BSA leads to a mixed oxide layer (CuO, Cu_2O, $Ni(OH)_2$) with a lower thickness (∼10 nm). Thus, the protein induces a decrease of the dissolution rate at E_{corr} and hence a decrease of the amount of redeposited Cu_2O and of the oxide layer thickness.

Key words: Copper alloy / seawater / protein adsorption / EIS / XPS / ToF-SIMS

Résumé – Effet de l'adsorption de BSA sur les couches d'oxydes développées sur l'alliage Cu70-Ni30 en eau de mer artificielle statique. Les alliages de cuivre habituellement utilisés dans les circuits de refroidissement de centrales électriques peuvent être affectés par la biocorrosion induite par la formation d'un biofilm. L'objectif global de ce travail est d'étudier l'influence de l'adsorption de biomolécules, qui est l'étape initiale de formation du biofilm, sur le comportement électrochimique de l'alliage 70Cu-30Ni (% massiques) et sur la composition chimique des couches d'oxydes. Dans ce travail, la biomolécule choisie est l'albumine de sérum bovin (BSA, protéine modèle) et des mesures électrochimiques réalisées après 1 h d'immersion en eau de mer artificielle statique ont été combinées à des analyses de surface. En présence de BSA, la résistance de transfert de charge estimée par impédance électrochimique (EIS) à E_{corr} est plus élevée, correspondant à un courant de corrosion plus faible. Sans BSA, deux couches d'oxydes sont mises en évidence par XPS et ToF-SIMS : une couche externe principalement composée d'oxyde de cuivre (couche de redéposition de Cu_2O) et une couche interne principalement composée de nickel oxydé (épaisseur globale : ∼30 nm). La présence de BSA conduit à une couche mixte d'oxydes (CuO, Cu_2O, $Ni(OH)_2$), d'épaisseur plus faible (∼10 nm). Ainsi, la protéine induit une diminution de la vitesse de dissolution à E_{corr} et, par conséquent, une diminution de la quantité de Cu_2O redéposé et de l'épaisseur de la couche oxydée.

Mots clés : Alliage de cuivre / eau de mer / adsorption de protéine / EIS / XPS / ToF-SIMS

* This article is based on the contribution presented at the "XIème Forum Biodétérioration" (4–5 June, 2012, École Nationale Supérieure des Mines de Saint-Étienne). The symposium was organised by the "Biodétérioration des Matériaux" commission, in collaboration with the "Construction–Bâtiment" commission of the CEFRACOR.

[1] Laboratoire de Physico-Chimie des Surfaces, UMR 7045 CNRS-ENSCP, Chimie ParisTech, 11 rue Pierre et Marie Curie, 75005 Paris, France
[2] Laboratoire Interfaces et Systèmes Électrochimiques, UPR 15 CNRS, Université Pierre et Marie Curie, 4 place Jussieu, 75252 Paris Cedex 05, France
isabelle.frateur@upmc.fr

1 Introduction

Power plants require cooling circuits with water as the cooling agent; therefore, they are generally located on seacoasts owing to the ready availability of abundant seawater. Tubes are the basic components of heat exchangers; they provide the heat transfer surface between one fluid flowing inside the tubes and other fluid flowing outside the tubes [1]. In cooling circuits, the water is usually circulating but some parts inside the tubes where water is stagnant may be found, depending also on operation time; therefore, hydrodynamics is one of the parameters to be studied.

Copper and copper alloys are commonly used in condensers and heat exchangers due to their high thermal conductivity, good resistance to corrosion and good mechanical workability. Cu-Ni alloys are preferred in marine environments because of their corrosion resistance due to the formation of a thin, adherent, protective surface film which forms naturally and quickly upon exposure to clean seawater. That surface film is complex and predominantly made up of cuprous oxide, often containing nickel and iron oxides, cuprous hydroxychloride and cupric oxide [2].

Cooling circuits of industrial plants are ideal incubators for microorganisms because they offer plenty of water, are maintained at temperatures between 30 °C to 60°, at pH of 6 to 9, have good aeration and provide a continuous source of nutrients, such as inorganic or organic compounds. The microorganisms present in cooling water circuits can be divided into planktonic or sessile cells. Sessile ones attach to surfaces and form what is known as biofilm. The development of a biofilm is considered to be a multistage process involving the following major steps: (a) formation of an organic conditioned film on the solid surface by adsorption of biomolecules such as proteins [3]; (b) transport of microorganisms from the water to the surface; (c) adhesion of microorganisms onto the surface; (d) replication of the attached cells and production of exopolymers; (e) detachment of parts of the biofilm that are swept along by the flowing water to repeat the process of biofilm formation elsewhere [4]. Biofouling is a consequence of biofilm formation; the significant negative effects of biofouling are the blockage of water free flow in the cooling circuit and consequent mechanical damage to pumps, clogging of condenser tubes, reduction of the heat transfer efficiency and microbially induced corrosion (MIC) also called biocorrosion [5]. Cu-Ni alloys have also shown good resistance to biofouling; the reason for the antifouling behaviour of these alloys is still not fully understood but the protective surface film should play a role [6].

There are two opposite goals for the control of microbial adhesion and biofilm formation: one is the prevention of biofilms, and the other one is their promotion. Controlling the adsorption of biomolecules, which is the first step in biofilm formation, by modifying the surface properties of the material may represent a good strategy for inhibiting microbial growth [7]. The global objective of this work was to study the influence of biomolecules adsorption on the electrochemical behaviour of 70Cu-30Ni (wt. %) alloy and the chemical composition of oxide layers, in different hydrodynamics conditions ((i) stagnant conditions; (ii) under flow and stirring of the solution; and (iii) using a rotating ring electrode). In this work, the chosen biomolecule was the bovine serum albumin (BSA), a model protein often used to study the protein-surface interactions due to its low cost and to a good knowledge of its properties [8,9]. Electrochemical measurements (corrosion potential (E_{corr}) vs. time, polarization curves and electrochemical impedance spectroscopy (EIS)) performed in static artificial seawater (ASW) during the very first steps of oxide layers formation (1 h immersion time) were combined to surface analyses by X-ray photoelectron spectroscopy (XPS) and time-of-flight secondary ion mass spectrometry (ToF-SIMS).

2 Experimental

2.1 Samples and solution

The samples provided by RSE S.p.A. were cut from real condenser tubes, and then flattened at Chimie ParisTech. Before each experiment, samples were mechanically polished with SiC papers down to grade 1200, then degreased in an ultrasonic bath three times in acetone for 5 min, once in ethanol for 10 min, and once in water for 10 min, dried under an argon flow, and finally exposed to UV for 15 min.

The solution under study was aerated artificial seawater (ASW; composition (g/L): NaCl (24.615), KCl (0.783), Na_2SO_4 (4.105), $MgCl_2(H_2O)_6$ (11.060), $CaCl_2$ (1.160), $NaHCO_3$ (0.201); pH = 8.0; ionic strength = 0.7155 M), without and with 20 mg.L^{-1} of BSA.

2.2 Electrochemical measurements

The electrochemical measurements were performed with a three-electrode cell, designed and manufactured at Chimie ParisTech, with the material to be studied (70Cu-30Ni alloy) as the working electrode, a platinum wire as the counter-electrode, and a saturated calomel electrode (SCE) as the reference electrode. Experiments were carried out at room temperature and in stagnant conditions (static working electrode and solution).

The corrosion potential (E_{corr}) was followed during the first hour of immersion, then cathodic or anodic polarization curve was plotted separately starting from +20 or –20 mV vs. E_{corr}, respectively, using a scan rate of 0.5 mV.s^{-1}. Electrochemical impedance diagrams were plotted at E_{corr} after 1 h of immersion, with a frequency domain ranging from 10^5 Hz to 10^{-3} Hz, 7 points per decade, and an amplitude of 10 mV peak-to-peak. Electrochemical measurements were collected by means of an EC-Lab SP-200 system from Bio-Logic.

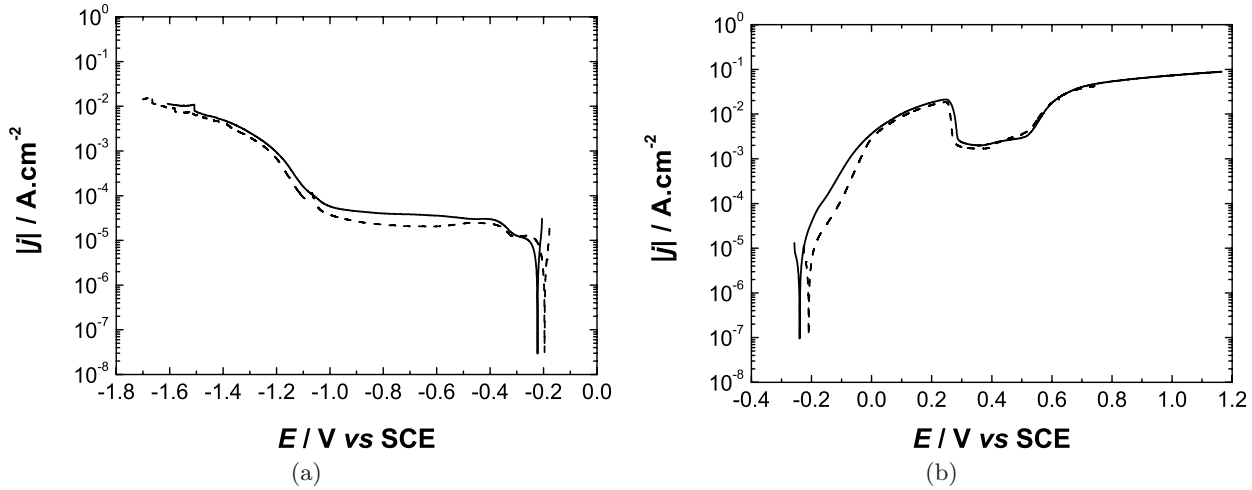

Fig. 1. (a) Cathodic and (b) anodic polarization curves of 70Cu-30Ni after 1 h of immersion at E_{corr} in aerated artificial seawater, (—) without BSA, and (– – –) with 20 mg.L^{-1} of BSA. Scan rate: 0.5 mV.s^{-1}.

Fig. 1. Courbes de polarisation (a) cathodiques et (b) anodiques de 70Cu-30Ni après 1 h d'immersion à E_{corr} en eau de mer artificielle aérée, (—) sans BSA et (– – –) avec 20 mg.L^{-1} de BSA. Vitesse de balayage : 0,5 mV.s^{-1}.

2.3 Surface analyses

Three 70Cu-30Ni samples were analyzed by XPS then by ToF-SIMS: (1) after polishing; (2) after 1 h of immersion at E_{corr} in ASW without BSA; and (3) after 1 h of immersion at E_{corr} in ASW with BSA. After the electrochemical measurements, the samples were gently dipped in ultra-pure water three times to remove the BSA molecules loosely bound to the surface, then dried with nitrogen before introduction in the fast-entry lock chamber of the XPS spectrometer.

XPS analyses were performed with a Thermo Electron Escalab 250 spectrometer, using a monochromatised Al Kα X-ray source (1486.6 eV). The analyser pass energy was 100 eV for survey spectra and 20 eV for high resolution spectra. The spectrometer was calibrated using Au $4f_{7/2}$ at 84.1 eV. The following core levels were recorded: Cu 2*p* (and Auger lines), Ni 2*p*, O 1*s*, C 1*s*, and N 1*s*. All spectra were referred to the C 1*s* peak for the carbon involved in C-C and C-H bonds, located at 285 eV The fitting of the complex C 1*s* signal was based on some published data [10]. Curve fitting of the spectra was performed with the Thermo Electron software "Avantage". The inelastic mean free path values were calculated by the TPP2M formula [11], and the photoemission cross-sections were taken from Scofield [12].

ToF-SIMS analyses were acquired using a ToF-SIMS V spectrometer (ION-TOF GmbH). The analysis chamber was maintained at less than 10^{-9} Pa in operation conditions. The depth profiles were performed using the instrument in dual beam mode. A pulsed 25 keV Bi^+ primary ion source (LMIG) at a current of 1.2 pA (high mass resolution mode), rastered over a scan area of 100×100 μm^2, was used as the analysis beam. The sputtering was performed using a 1 keV Cs^+ ion beam at a current of 50 nA, and rastered over an area of 300×300 μm^2. The depth profiles were obtained in negative polarity meaning only negative ions were analysed The distribution of the ionized fragments, all measured simultaneously, were plotted versus Cs^+ ion sputtering time. The intensity was reported using a logarithmic scale, which gave equal emphasis to signals of all intensities. The variation of the ion intensity with sputtering time reflects the variation of the in-depth concentration but is also dependent on the matrix from which the ions are emitted. Data acquisition and processing were performed using the IonSpec software.

3 Results

3.1 Electrochemical measurements

During the first hour of immersion, the corrosion potential E_{corr} decreases till reaching a steady-state value of -0.23 ± 0.01 V vs. SCE without BSA. The presence of 20 mg.L^{-1} of BSA induces a more anodic E_{corr} value (-0.20 ± 0.01 V vs. SCE i.e. difference of $\sim$0.03 V with the value found without protein).

Figure 1a shows the cathodic polarization curves obtained without and with 20 mg.L^{-1} of BSA. The wide plateau observed for potentials ranging from –0.40 to –1.00 V vs. SCE illustrates the reduction of dissolved oxygen:

$$O_2 + 2H_2O + 4e^- \rightarrow 4OH^- \quad \text{at pH 8.0} \qquad (1)$$

The corresponding current density is divided by 2 in the presence of the protein ($|j| \sim 40$ μA.cm^{-2} without BSA to be compared to $|j| \sim 20$ μA.cm^{-2} with BSA). This difference in plateau current is not necessarily due to the BSA but may also be induced by a difference in natural convection.

The short current plateau observed between –0.25 and –0.30 V vs. SCE ($|j| \sim 10$ μA.cm^{-2}) may illustrate the

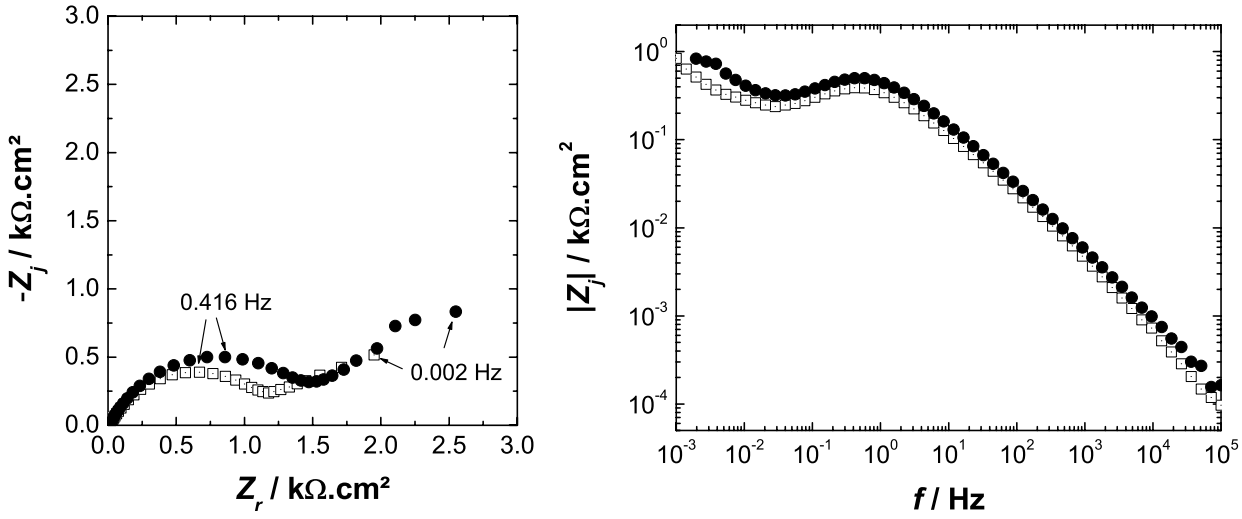

(a) (b)

Fig. 2. Impedance diagrams of 70Cu-30Ni plotted at E_{corr} after 1 h of immersion in aerated artificial seawater, (⊡) without and (●) with 20 mg.L^{-1} of BSA. (a) Complex plane plot, and (b) imaginary part of the impedance as a function of frequency.
Fig. 2. Diagrammes d'impédance de 70Cu-30Ni tracés à E_{corr} après 1 h d'immersion en eau de mer artificielle aérée, (⊡) sans et (●) avec 20 mg.L^{-1} de BSA. (a) Diagrammes de Nyquist et (b) partie imaginaire de l'impédance en fonction de la fréquence.

first step of dissolved oxygen reduction with production of H_2O_2 [13,14]:

$$O_2 + 2H_2O + 2e^- \rightarrow H_2O_2 + 2OH^- \quad \text{at pH 8.0} \qquad (2)$$

The anodic polarization curves obtained without and with 20 mg.L^{-1} of BSA are presented in Figure 1b. In the absence of protein, the anodic polarization curves show very high dissolution currents. In particular, a pseudo-plateau, corresponding to a current density of ∼2.5 mA.cm^{-2}, can be observed between 0.30 and 0.50 V vs. SCE; therefore, this plateau current is not a passive current, and hence the oxide film formed on the surface is not a passive layer. Moreover, visual observation of the electrode surface after an anodic scan shows a green layer, the thickness of which increases with the end anodic potential. This green layer corresponding to high anodic currents may be formed by redeposition due to the saturation of the solution in copper ions. No influence of the BSA on the anodic electrochemical behaviour can be seen. However, after the anodic polarization curve, the green color is no more observed for the alloy surface in the presence of BSA.

Figure 2a shows the impedance diagrams in the complex plane plotted at E_{corr} after 1 h of immersion in aerated artificial seawater, without protein and with 20 mg.L^{-1} of BSA. The diagrams exhibit two capacitive loops: one high frequency (HF) depressed semi-circle, and a low frequency (LF) loop forming an angle of ∼45 °C with the X-axis that illustrates mass transport (Warburg-like impedance). The size of the HF loop is slightly increased in the presence of BSA.

In Figure 2b, the imaginary part of the impedance (Z_j) is plotted as a function of the frequency (f) in logarithmic coordinates. In the HF range, a straight line with a slope lower than 1 in absolute value can be observed, evidencing a constant-phase-element (CPE) behavior. The impedance of a CPE is given by:

$$Z_{CPE}(\omega) = \frac{1}{Q(j\omega)^{\alpha}} \qquad (3)$$

with $\omega = 2\pi f$. The CPE parameters α and Q can be obtained from the graphical methods presented by Orazem et al. [15]. The parameter α is calculated from the slope of the log $|Z_j|$ vs. log f curve:

$$\alpha = \left| \frac{\mathrm{d}\log|Z_j(f)|}{\mathrm{d}\log f} \right| \qquad (4)$$

and Q is obtained from:

$$Q = -\frac{1}{Z_j(f)(2\pi f)^{\alpha}} \times \sin\left(\frac{\alpha\pi}{2}\right). \qquad (5)$$

The parameters α and Q obtained by graphical evaluation of equations (4) and (5) are the same as would be obtained by regression analysis. The α and Q values for the impedance diagrams shown in Figure 2 are given in Table 1.

If this CPE behavior is assumed to be associated with surface distributed time constants for charge-transfer reactions (time-constant distribution along the electrode surface), then it is possible to apply the equation derived by Brug et al. to calculate the effective capacitance associated with the CPE [16,17]:

$$C_{eff} = Q^{1/\alpha}\left(R_e^{-1} + R_t^{-1}\right)^{(\alpha-1)/\alpha} \qquad (6)$$

where R_e is the electrolyte resistance and R_t the charge transfer resistance. The capacitance values extracted from the impedance diagrams shown in Figure 2, of the order

Table 1. CPE parameters extracted from the impedance diagrams presented in Figure 2 by graphical evaluation of equations (4) and (5) [15], electrolyte and charge transfer resistances estimated by fitting the $R_e - (R_t//\mathrm{CPE}_{dl})$ equivalent circuit to the HF loop, and effective capacitance associated with the CPE calculated from equation (6).

Tableau 1. Paramètres CPE extraits par analyse graphique des diagrammes d'impédance présentés sur la figure 2 (Éqs. (4) et (5)) [15], résistances d'électrolyte et de transfert de charge estimées par ajustement de la boucle HF par le circuit équivalent $R_e - (R_t//\mathrm{CPE}_{dl})$ et capacité équivalente associée au CPE calculée à partir de l'équation (6).

	α	Q/F.cm^{-2}.s$^{(\alpha-1)}$	R_e/Ω.cm^2	R_t/Ω.cm^2	C_{eff}/F.cm^{-2}
Without BSA	0.82	1.67×10^{-04}	12.0	1197	43×10^{-06}
With BSA	0.75	2.39×10^{-04}	11.8	1565	34×10^{-06}

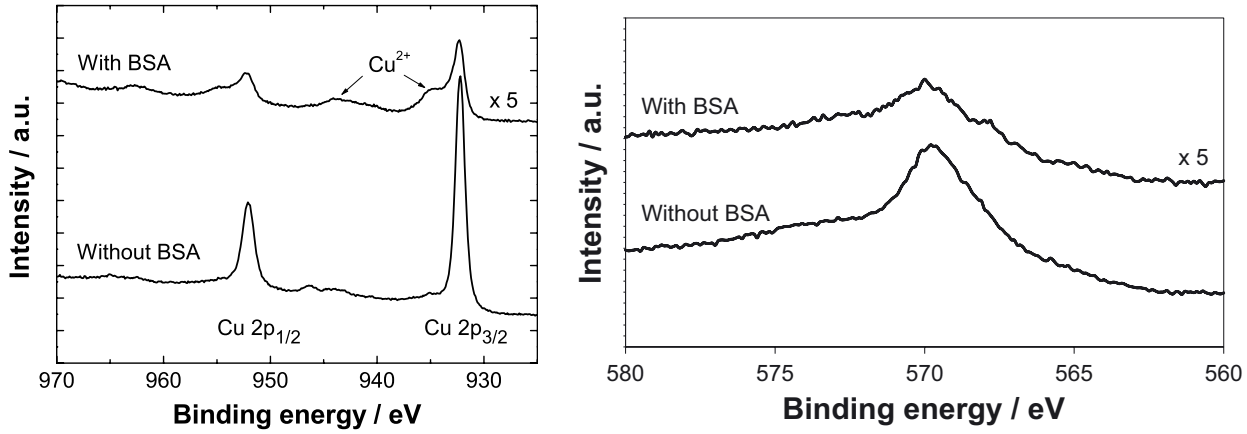

Fig. 3. (a) XPS Cu 2*p* core level spectra and (b) Cu $L_3M_{45}M_{45}$ Auger lines of 70Cu-30Ni after 1 h of immersion at E_{corr} in aerated artificial seawater without and with 20 mg.L^{-1} of BSA.

Fig. 3. (a) Spectres XPS des niveaux de cœur Cu 2p et (b) raie Auger Cu $L_3M_{45}M_{45}$ pour 70Cu-30Ni après 1 h d'immersion à E_{corr} en eau de mer artificielle aérée sans et avec 20 mg.L^{-1} de BSA.

of several tens of μF.cm^{-2} (Tab. 1), are typical of those for a double layer capacitance (C_{dl}). Hence, the HF loop illustrates charge transfer and can be represented by the $R_t//\mathrm{CPE}_{dl}$ equivalent circuit; its diameter is equal to R_t.

In the presence of BSA, R_t is 1.4 times higher than without protein. This indicates that albumin leads to a decrease of the corrosion current (inversely proportional to R_t), and hence of the corrosion rate.

3.2 Surface analyses

For the sample after polishing, it is observed from XPS and ToF-SIMS data (not shown here) a mixed copper oxides (Cu_2O and CuO) and nickel hydroxide ($Ni(OH)_2$) layer, with a thickness of ~1.3 nm and the following atomic composition: 43 at. % Cu_2O + 25 at. % CuO + 32 at. % $Ni(OH)_2$. An enrichment in copper of the alloy beneath the oxide layer is also detected (77 at. % Cu + 23 at. % Ni to be compared to 68 at. % Cu + 32 at. % Ni for the bulk alloy).

Differences in chemical composition and thickness of the oxide layers are shown without and with BSA.

After immersion in the BSA-free ASW, the XPS Cu $2p_{3/2}$ core level peak with a binding energy located at 932.3 eV (Fig. 3a) and the Cu Auger line ($L_3M_{45}M_{45}$) at a binding energy of 570.2 eV (Fig. 3b) demonstrate only the presence of Cu^+ (no Cu^{2+} as for the sample after polishing) [18].

From the XPS Ni $2p_{3/2}$ core level spectrum with a peak located at 856.1 eV and the corresponding satellite at 861.7 eV, the presence of $Ni(OH)_2$ in the surface layer is shown (Fig. 4) [19]. The atomic composition of this oxide film calculated from XPS data (93 at. % Cu_2O + 7 at. % $Ni(OH)_2$) indicates a Cu_2O-rich layer. It is important to mention that the depth analyzed by XPS is about 10 nm.

A characteristic ToF-SIMS negative depth profile obtained with 70Cu-30Ni alloy immersed during 1 h at E_{corr} in ASW without BSA is presented in Figure 5. This profile allows evidencing a possible stratification of the different compounds on the alloy surface. It shows four regions. A first one that extends from 0 s to 10 s of sputtering characterized by an increase of all signals and corresponding to the time necessary to reach a steady state. After 10 s, one enters the second region that extends up to 200 s of sputtering. This region is characterized by an intense CuO_2^- signal. As soon as one probes deeper into this region, a progressive increase of the NiO_2^- signal is observed. This indicates that the outer surface layer is mainly composed of copper oxide, with the presence of some Ni oxide and/or hydroxide, in agreement with XPS data. In the third region that extends from 200 s to 290 s, a sharp decrease of

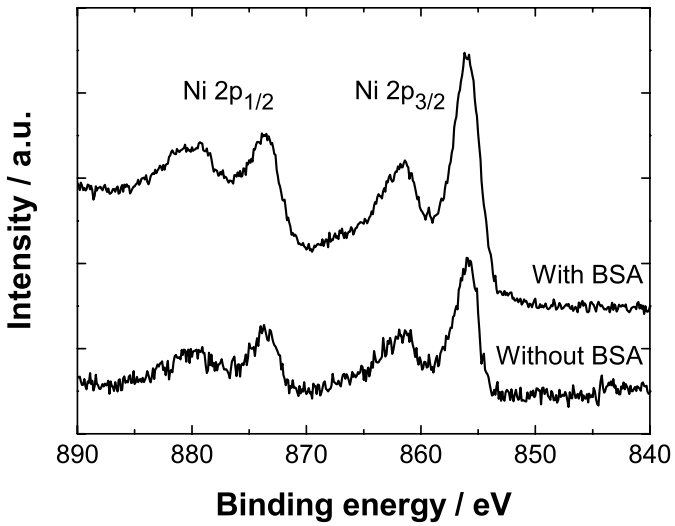

Fig. 4. XPS Ni 2*p* core level spectra of 70Cu-30Ni after 1 h of immersion at E_{corr} in aerated artificial seawater without and with 20 mg.L^{-1} of BSA.

Fig. 4. Spectres XPS des niveaux de cœur Ni 2p pour 70Cu-30Ni après 1 h d'immersion à E_{corr} en eau de mer artificielle aérée sans et avec 20 mg.L^{-1} de BSA.

the CuO_2^- signal and a very intense NiO_2^- signal are observed. This region is assigned to the formation of a nickel oxide and/or hydroxide inner layer in which the presence of oxidized copper cannot be excluded. Finally, after 290 s of sputtering, one enters the fourth region characterized by a sharp decrease of all oxidized signals ($18O^-$, CuO_2^- and NiO_2^-) and a constant and intense plateau for the Ni_2^- signal that is characteristic of the metallic substrate.

From the ToF-SIMS depth profiles, it can be concluded that in the absence of BSA two oxidized layers can be observed: a 18 nm-thick outer layer mainly composed of copper oxide and a 12 nm-thick inner layer mainly composed of nickel oxide and/or hydroxide, with a global thickness of ∼30 nm. To convert a sputtering time into an oxide layer thickness, the theoretical sputtering rates of the pure metallic substrates were used (values given in tables in the same sputtering conditions). In our case, the thickness of the outer layer was estimated from the sputtering rate of pure metallic Cu, and that of the inner layer was estimated from the sputtering rate of pure metallic Ni.

After immersion in the BSA-containing solution, the XPS Cu $2p_{3/2}$ core level spectrum exhibits three peaks (Fig. 3a): one located at 932.3 eV attributed to Cu^0 and/or Cu^+, another one with a binding energy located at 934.5 eV and the corresponding satellite at higher binding energy attributed to Cu^{2+}. Moreover, the Cu Auger line at a binding energy of 570.0 eV (Fig. 3b) indicates that the Cu 2*p* peak at 932.3 eV is associated to Cu^+. The XPS Ni $2p_{3/2}$ core level spectrum recorded in the presence of BSA exhibits the same features as without protein: a peak at a binding energy of 856.0 eV and the corresponding satellite at 861.6 eV showing the presence of $Ni(OH)_2$ in the surface layer (Fig. 4). From these XPS data, it can be concluded that the presence of BSA leads to a mixed copper oxides (CuO and Cu_2O) and nickel hydroxide layer, with the following atomic composition: 11 at. % Cu_2O + 44 at. % CuO + 45 at. % $Ni(OH)_2$. A lower amount of Cu_2O and higher amounts of CuO and $Ni(OH)_2$ are detected compared to the results obtained in the absence of BSA.

By ToF-SIMS, it is not possible to identify a stratification of the different compounds on the alloy surface in the presence of the protein. Thus, depth profiles show one mixed oxide layer (oxidized copper and nickel) with a lower thickness of ∼10 nm. In that case, the sputtering time was converted into an oxide layer thickness by using an average sputtering rate equal to the sum of the sputtering rates of pure metallic Cu and Ni weighted by the fractions of the two elements in the alloy (i.e. sputtering rate of Cu+Ni oxide = 0.7 × sputtering rate of metallic Cu + 0.3 × sputtering rate of metallic Ni).

The N 1*s* spectrum recorded after immersion in ASW with BSA (Fig. 6a) exhibits a major symmetric peak, centered at 400.2 eV, as expected for the amine or amide groups of BSA [20]. The C 1*s* signal obtained in the same conditions is shown in Figure 6b. It can be fitted with three contributions corresponding to well identified carbon bonds present in the BSA molecule: C1, at a binding energy of 285.0 eV, assigned to C-C and C-H; C2, at a binding energy of 286.4 eV, attributed to C-N and C-O single bonds; and C3, at a binding energy of 288.3 eV, assigned to O=C-O and O=C-N (peptide bonds) bonds [10].

From the N 1*s* and C 1*s* signals, it is possible to calculate different "nitrogen/carbon" or "carbon/carbon" atomic ratios. The values of these ratios obtained for the 70Cu-30Ni alloy immersed in ASW without and with BSA, as well as those estimated in previous studies for the BSA powder [10, 21] are presented in Table 2. The good agreement between the values for the sample put into contact with the BSA and the BSA powder provides a fingerprint for the protein, and allows us to conclude that the protein is present on the surface The thickness estimated from XPS data for this adsorbed layer is ∼3 nm, which corresponds to one monolayer [9].

4 Discussion

After short-term immersion (1 h of exposure) at E_{corr} in ASW without BSA, combined XPS and ToF-SIMS data show two oxidized layers: an outer layer mainly composed of cuprous oxide (Cu_2O) and an inner layer mainly composed of oxidized nickel. Thus, the surface layers can be depicted by the model presented in Figure 7a. The presence of BSA leads to a mixed oxide layer composed of CuO, Cu_2O, and $Ni(OH)_2$ (Fig. 7b). Compared to the results obtained without BSA, there is a marked decrease of the Cu_2O content in the oxide layer, and its thickness is lower (∼10 nm).

On the other hand, impedance diagrams exhibit a LF loop illustrating mass transport (diffusion convection

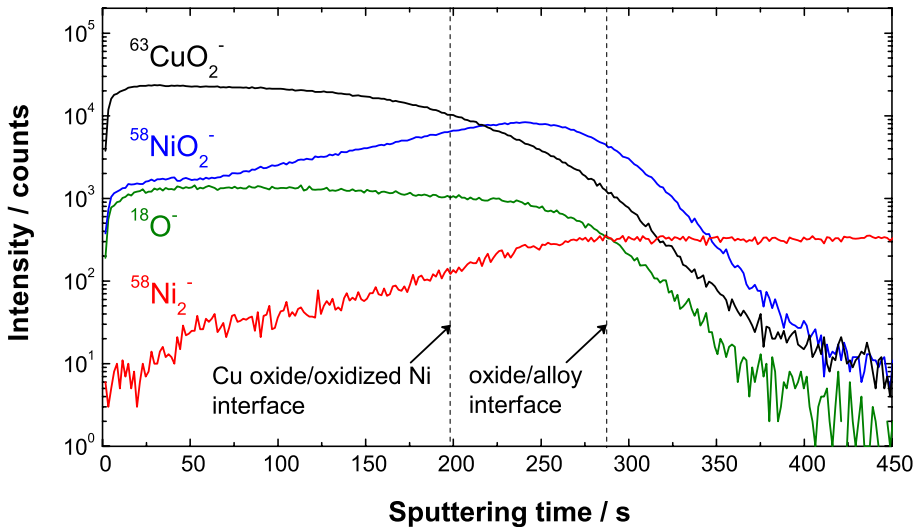

Fig. 5. Characteristic ToF-SIMS negative depth profile of 70Cu-30Ni after 1 h of immersion at E_{corr} in aerated artificial seawater without BSA.

Fig. 5. Profils ToF-SIMS en mode négatif de 70Cu-30Ni après 1 h d'immersion à E_{corr} en eau de mer artificielle aérée sans BSA.

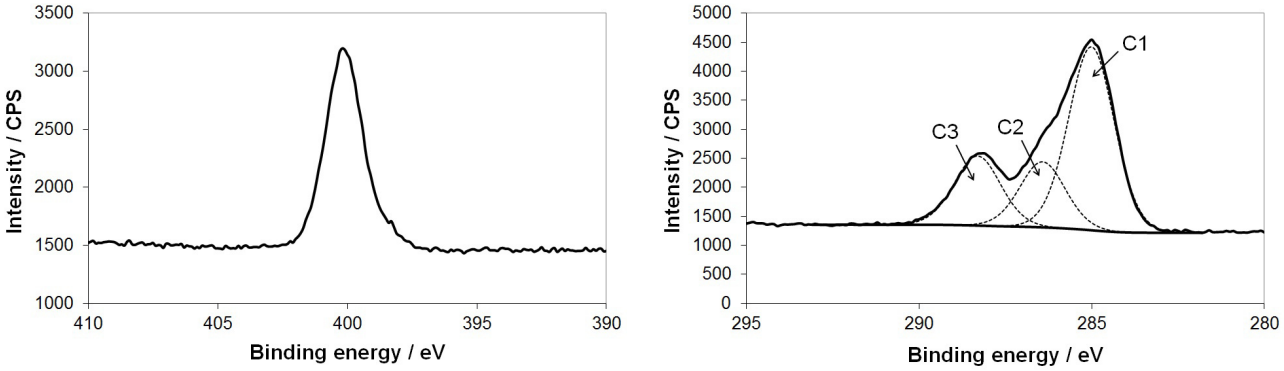

(a) (b)

Fig. 6. XPS (a) N 1*s* and (b) C 1*s* core level spectra of 70Cu-30Ni after 1 h of immersion at E_{corr} in aerated artificial seawater with 20 mg.L^{-1} of BSA. Solid line: experimental spectra; dashed line: peak decomposition.

Fig. 6. Spectres XPS des niveaux de cœur (a) N 1s et (b) C 1s pour 70Cu-30Ni après 1 h d'immersion à E_{corr} en eau de mer artificielle aérée avec 20 mg.L^{-1} de BSA. Trait plein : spectres expérimentaux ; trait pointillé : décomposition.

Table 2. Atomic ratios calculated from the XPS N 1*s* and C 1*s* core level spectra recorded for the BSA powder, and for 70Cu-30Ni after 1 h of immersion at E_{corr} in aerated artificial seawater without and with 20 mg.L^{-1} of BSA.

Tableau 2. Rapports atomiques calculés à partir des spectres XPS des niveaux de cœur N 1s et C 1s enregistrés pour la poudre de BSA et pour 70Cu-30Ni après 1 h d'immersion à E_{corr} en eau de mer artificielle aérée sans et avec 20 mg.L^{-1} de BSA.

	N/Ctotal	N/(C2+C3)	C1/Ctotal	C2/Ctotal	C3/Ctotal
BSA powder	0.22	0.48	0.54	0.26	0.20
ASW	0.03	0.14	0.78	0.13	0.09
ASW+BSA	0.20	0.45	0.56	0.22	0.22

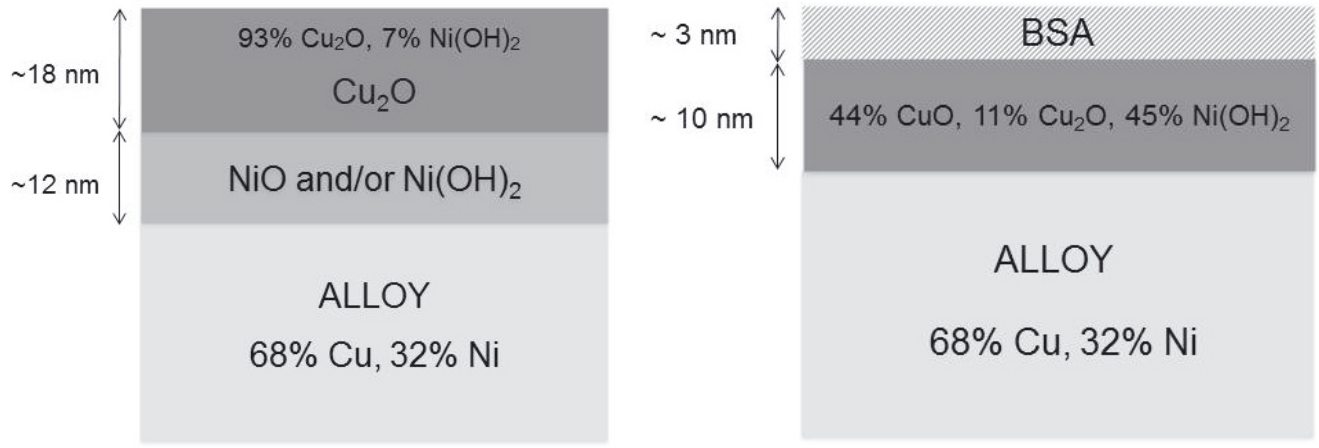

(a) (b)

Fig. 7. Models of the surface layers deduced from combined XPS and ToF-SIMS results for 70Cu-30Ni after 1 h of immersion at E_{corr} in aerated artificial seawater (a) without and (b) with 20 mg.L^{-1} of BSA.

Fig. 7. Modèles des couches de surface déduits de la combinaison des résultats XPS et ToF-SIMS pour 70Cu-30Ni après 1 h d'immersion à E_{corr} en eau de mer artificielle aérée (a) sans et (b) avec 20 mg.L^{-1} de BSA.

impedance) and show lower corrosion current in the presence of the protein.

It is accepted by many authors that the corrosion of copper alloys is controlled by mass transport processes to and from corroding surfaces, involving O_2, Cl^-, OH^-, Cu^+ and $CuCl_2^-$ species [22]. The anodic reactions involve:

$$Cu \rightarrow Cu^+ + e^- \quad (7)$$

followed by the formation of the cuprous complex:

$$Cu^+ + 2Cl^- \rightarrow CuCl_2^- \quad (8)$$

Then, cuprous oxide can be formed from $CuCl_2^-$ as follows [13]:

$$2CuCl_2^- + 2OH^- \rightarrow Cu_2O + H_2O + 4Cl^- \quad (9)$$

Moreover, there are basically two mechanisms of de-alloying for binary alloys proposed in the literature [13]:

(1) simultaneous dissolution of both components of the alloy followed by redeposition of one component (usually the more noble one);
(2) selective dissolution of one element from the alloy.

Beccaria and Crousier studied the de-alloying of Cu-Ni alloys exposed to natural seawater for 660 h and found simultaneous dissolution of both components with possible redeposition of copper for nickel contents lower than 50%, whereas for nickel concentrations higher than 50% selective dissolution of copper took place [23]. Results obtained by Mansfeld et al. for long-term exposure (1–3 months) to natural seawater suggest that de-alloying of 70Cu-30Ni is initially due to simultaneous dissolution of copper and nickel and subsequent redeposition of copper in agreement with the results of Beccaria and Crousier [13].

Our results obtained for short-term exposure to ASW are in agreement with the conclusions drawn by Beccaria and Crousier, and Mansfeld et al.; the cuprous oxide Cu_2O detected on the surface by XPS and ToF-SIMS is formed by redeposition of dissolved copper.

The combination of electrochemical measurements and surface analyses allows us to conclude that in stagnant conditions the BSA leads to a decrease of the dissolution rate at E_{corr} and hence a decrease of the amount of redeposited Cu_2O and of the oxide layer thickness.

5 Conclusions

The influence of BSA adsorption on the electrochemical behavior of 70Cu-30Ni alloy and the chemical composition of oxide layers was studied in static artificial seawater by combined electrochemical measurements and surface analyses.

From polarization curves, high anodic dissolution currents were shown (no passive current). The BSA had a slight effect on the electrochemical behavior of the copper alloy. Thus, E_{corr} value after 1 h of immersion was ~30 mV more anodic with BSA, and EIS measurements indicated a decrease of the corrosion current induced by the protein.

From XPS and ToF-SIMS analyses, different surface chemical compositions of 70Cu-30Ni were shown without and with BSA. In the absence of BSA, two oxidized layers were observed: an outer layer mainly composed of copper oxide (Cu_2O redeposited layer) and an inner layer mainly composed of oxidized nickel, with a global thickness of ~30 nm. In the presence of BSA, the protein was detected on the surface and the thickness of the adsorbed layer was ~3 nm, corresponding to one monolayer. The presence of BSA led to a mixed oxide layer (CuO, Cu_2O, $Ni(OH)_2$) with a lower thickness (~10 nm).

The combination of electrochemical measurements and surface analyses allows us to conclude that the BSA

induces a decrease of the dissolution rate at E_{corr} and hence a decrease of the amount of redeposited Cu_2O and of the oxide layer thickness.

Acknowledgements. The research leading to these results has received funding from the European Community's Seventh Framework Programme (FP7/2007-2013) under grant agreement No. 238579. Project website: www.biocor.eu/ip8 (RSP3).

References

[1] M.J. Fernandez Torres, F. Ruiz Bevia, *J. Clean. Prod.* **26** (2012) 1-8

[2] C.A. Powell, H.T. Michels, Copper-Nickel Alloys for seawater corrosion resistance and antifouling – A state of the art review, Corrosion 2000, NACE March 2000 (© NACE)

[3] G.T. Taylor, P.J. Troy, S.K. Sharma, *Mar. Chem.* **45** (1994) 15-30

[4] S.G. Choudhary, *Hydrocarb. Process.* **77** (1998) 91-102

[5] S. Rajagopal, K.V.K. Nair, J. Azariah, G. van der Velde, H.A. Jenner, *Mar. Environ. Res.* **2** (1996) 201-221

[6] A.M. Alfantazi, T.M. Ahmed, D. Tromans, *Mater. Design* **30** (2009) 2425-2430

[7] K. Hori, S. Matsumoto, *Biochem. Eng. J.* **48** (2010) 424-434

[8] T. Peters, Serum albumin, *Adv. Protein Chem.* **37** (1985) 161-245

[9] D.C. Carter, J.X. Ho, *Adv. Protein Chem.* **45** (1994) 153-205

[10] I. Frateur, J. Lecœur, S. Zanna, C.-O.A. Olsson, D. Landolt, P. Marcus, *Electrochim. Acta* **52** (2007) 7660-7669

[11] S. Tanuma, C.J. Powell, D.R. Penn, *Surf. Interface Anal.* **17** (1991) 911-926

[12] J.H. Scofield, *J. Electron Spectrosc.* **8** (1976) 129-137

[13] F. Mansfeld, G. Liu, H. Xiao, C.H. Tsai, B.J. Little, *Corros. Sci.* **12** (1994) 2063-2095

[14] I. Frateur, Incidence de la corrosion des matériaux ferreux sur la demande en chlore libre en réseaux de distribution d'eau potable, Ph.D. Thesis, University of Paris 6, France, 1997

[15] M.E. Orazem, N. Pébère, B. Tribollet, *J. Electrochem. Soc.* **153** (2006) B129-B136

[16] B. Hirschorn, M.E. Orazem, B. Tribollet, V. Vivier, I. Frateur, M. Musiani, *Electrochim. Acta* **55** (2010) 6218-6227

[17] G.J. Brug, A.L.G. van den Eeden, M. Sluyters-Rehbach, J.H. Sluyters, *J. Electroanal. Chem.* **176** (1984) 275-295

[18] A. Galtayries, J.-P. Bonnelle, *Surf. Interface Anal.* **23** (1995) 171-179

[19] A. Machet, A. Galtayries, S. Zanna, L. Klein, V. Maurice, P. Jolivet, M. Foucault, P. Combrade, P. Scott, P. Marcus, *Electrochim. Acta* **49** (2004) 3957-3964

[20] Y.F. Dufrêne, T.G. Marchal, P.G. Rouxhet, *Appl. Surf. Sci.* **144-145** (1999) 638-643

[21] L. Lartundo-Rojas, Influence de l'adsorption de protéine (BSA) sur le comportement électrochimique et la composition de surface d'un alliage Fe-17Cr en solution aqueuse, Ph.D. Thesis, University of Paris 6, France, 2007

[22] O.E. Barcia, O.R. Mattos, N. Pébère, B. Tribollet, *J. Electrochem. Soc.* **10** (1993) 2825-2832

[23] A.M. Beccaria, J. Crousier, *Brit. Corros. J.* **24** (1989) 49-52